3D Assessment of Rainfall-induced Slope Movements and Risk Mitigation Strategies

Wei He
Geoinventions Consulting Services, Brisbane, Queensland 4119, AUSTRALIA
Wade.he@geoinventions.com.au

Barry Kok
Geoinventions Consulting Services, Brisbane, Queensland 4119, AUSTRALIA
Barry.kok@geoinventions.com.au

Sangmin Lee
Geoinventions Consulting Services, Brisbane, Queensland 4119, AUSTRALIA
Sangmin.lee@geoinventions.com.au

ABSTRACT

Abstract: Severe financial lost is induced due to rainfall-induced movements or shallow landslides of slopes which embed displacement-sensitive stuctures. The 2-step assessment&design procedure was proposed and practiced, based on strain-based 3D numerical method. On the basis of data collection and desk view, the regional rainfall intensity and duration is compared to the empirical landslides threshold in the first step. The risk level can be defined in the region to determine if strain-based design analysis is required. If it is in high-risk zone, the slope needs to be assessed in 3D by using fluid-solid fully-coupled Finite Element Method (FEM) in step 2. Remediation plan can be proposed to meet the design criteria. The required information such as empirical threshold of initiating shallow landslides, unsaturated soil parameters estimating method, and fluid-solid fully-coupled method were provided in this paper. A problematic slope in Brisbane area was assessed by following this procedure. A critical rainfall event (1 in 2000 AEP) of 150mm/day was applied on the slope surface. 1.114m superficial movement was observed in the 3D model, which corresponds well with measured movement onsite. The removal of colluvium in the potential moving area and drainage fingers were proposed to mitigate the risk and justified by further analysis.

Keywords: slope movement; rainfall; 3D modeling; finite element method (FEM); unsaturated soil

1 INTRODUCTION

Rainfall-induced slope movement caused severe financial lost due to the detrimental influence on embedded structures, such as pile foundation and pipelines (Fig.1). Comparing to other scenarios, a globally stable slope with certain level of movement in shallow depth can even damage these displacement-sensitive structures. However, this is a significant engineering problem which requires further study.

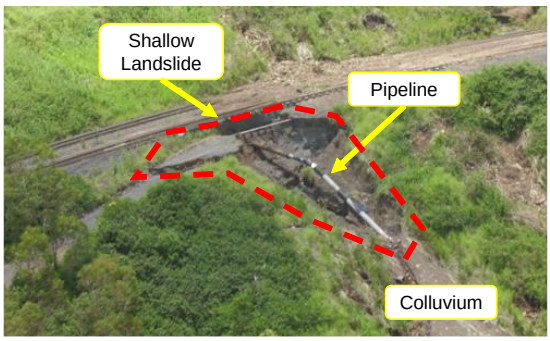

Fig. 1 A rainfall-induced slope slip with pipeline embedded in Queensland, Australia

Extensive attentions have been paid on rainfall-induced slope instability, due to numerous large-scale failure cases reported in world-wide (Caine, 1980; Brand, 1984; Au, 1998; Chen, 2005; Borja, 2010). The critical combination of rainfall intensity and its duration is revealed as the essential factors which trigger shallow landslides and debris flows (Zhan, 2014). The established intensity-duration curves are practical for forecasting the potential landslides, but these require well-recorded historical landslides database in different regions with various soil properties. For a specific site, engineering evaluations need to be on the basis of stability analysis. This can be carried out by introducing unsaturated seepage analysis into conventional equilibrium limit analysis (Fredlund, 2012; Muntohar, 2010; Sagitaningrum, 2017), or strength reduction method (Cai, 1998; Cho, 2001). However, these methods are insufficient for the prediction of the actual shallow movements. Due to the complexity of coupling effect, the most common approach to analyze rainfall-induced movement is to uncouple the fluid flow and slope-stability problem, and treat them in a sequential fashion instead (Borja,

2010). Recently, Jamei (2015) performed numerical analysis which took into account the fluid-solid coupled effect, but it did not consider 3D effect and may underestimate the problem.

Rainfall thresholds can be defined on physical (process-based, conceptual) or empirical (historical, statistical) bases (Guzzetti, 2007). In this paper, the procedure of evaluating the slope movement was proposed based on 3D fluid-solid fully coupled finite element method. A real case in Brisbane region was studied in detail to indicate the capability.

2 SLOPE RESPONSE UNDER RAINFALL EVENTS

2.1 Observed rainfall-induced slope movement in the literature

Few cases with measured slope movement due to rainfall events can be found in the literature, although a great number of landslides after heavy rainfall have been reported. Many studies revealed that the landslides had close correlation with rainfall events (Chen, 2004; Lateh, 2010). 69.4% of landslides in world wide were triggered by precipitation and infiltration as per the study in Europe (Pinto, 2011).

Table 1 Reported Rainfall-induced Slope Movement

Location	Rainfall Intensity (mm/d)	Moving Velocity (mm/d)	Reference
Wuhan, China	-	12	Chen, 2004
Calabria, Italy	90	100	Capparelli, 2010
Cameron Highland, Malaysia	60	100-140	Lateh, 2010
Beijing, China	30 (wet) 44 (dry)	6 (wet) 13 (dry)	Qian, 2011

Except for the instability cases, three site monitoring and one centrifugal test result, which recorded both rainfall intensity and movement development, have been tabulated in Table 1. A highway slope of 450m in extension and 50m in height was monitored in Wuhan, China, from May 2002 to January 2003 (Chen, 2004). The soil/rock encountered in the slope included 1.5-2.0m yellow clay, followed by 30m thick highly weathered silty mudstone, followed by sandstone. The drastic movement increase at the rate of approximately 12mm/day was observed in July 2002, which occurred immediately after a heavy rainfall event. However, no rainfall intensity and duration were reported. Capparellli reported a large debris slide monitoring in Calabria, Italy, between September 2009 and August 2010 (Capparelli, 2010). Before the monitoring plan, a shallow landslide was observed on 12 December in 2008, following an intensive rainfall event. Maximum superficial velocities of the slope reached a peak of 100mm/day at the beginning of the monitoring (30 January 2010), following a four-day intense rain (approximately 360mm). A theodolite study on slow hill-slope movement at Gunung Pass site of Cameron Highland district of Malaysia was conducted to monitor slope movement during two wet seasons in 2008 (Lateh, 2010). The monitoring results indicated that slope movement was accelerated by each heavy rainfall event. The maximum moving velocity was approximately 140mm/day during the wet season in November 2008 with rainfall intensity up to 60mm/day. Except for site investigation, centrifugal tests can also be adopted to study the rainfall-induced slope movement (Qian, 2011). Qian prepared two slope models with different initial water content. 52(70)-day rain of 30(44)mm/day in intensity was placed on a silty clay model slope, for wet(dry) model. The slope movement of 6mm/day in average was observed in the wet model, while that of 13mm/day in average was observed in the dry model.

The limited data indicated that the superficial movement of slope may reach the velocity of over 100mm/day, under rainfall of 60-90mm/day in intensity. Note that the available data are based on either convex hillslope or highway slope, which have less catchment area than a concave hillslope. Therefore, larger moving velocity may be observed in concave hillslopes, which are also preferable locations to embed pipelines.

2.2 Empirical rainfall thresholds for shallow landslides

Hundreds of rainfall events that resulted in landslides have been collected and analyzed by several researchers in various regions (Caine, 1998; Chen, 2005; Guzzetti, 2007). Empirical rainfall thresholds for the initiation of landslides were proposed in the form of intensity-duration curves. Soil properties and slope topography have not been considered in empirical thresholds. Thus, each curve needs to be adopted as a regional solution, or a lower bound threshold when the database is collected from world-wide.

According to literature, landslides basically fall into four types: shallow landslides, soil slip, debris flow and lahar. This paper focus on shallow landslides which may induce unacceptable displacement to embedded structures. Table 2 shows the available empirical thresholds which have taken shallow landslides into account. The threshold proposed for debris flow only in Indonesia is also included. The thresholds were plotted in Figure 2 for better illustration.

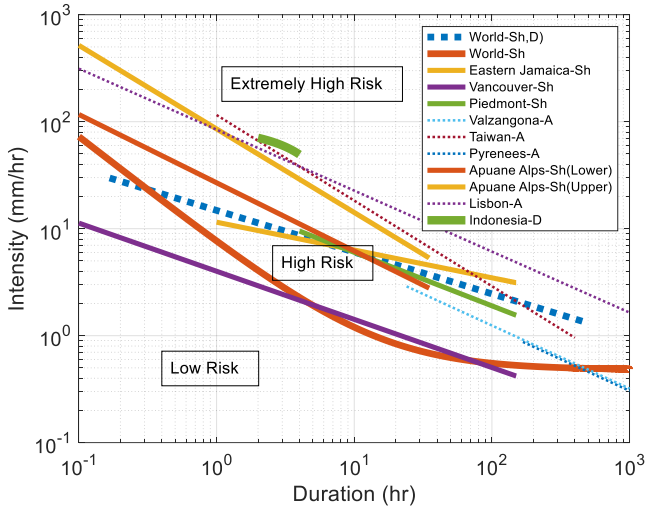

Fig. 2 Intensity – duration curves proposed for shallow landslides

Table 2 Intensity – duration thresholds for the initiation of shallow landslide

Area	type	Equation	Range of D, hr
World	Sh, D	$I = 14.82 \times D^{-0.39}$	0.167~500
World	Sh	$I = 0.48 + 7.2 \times D^{-1}$	0.1~1000
Eastern Jamaica	Sh	$I = 11.5 \times D^{-0.26}$	1~150
North Shore Mountains, Vancouver, Canada	Sh	$I = 4 \times D^{-0.45}$	0.1~150
Piedmont, NW Italy	Sh	$I = 19 \times D^{-0.5}$	4~150
Valzangona, N Apennines, Italy	A	$I = 18.83 \times D^{-0.59}$	24~3360
Taiwan	A	$I = 115.47 \times D^{-0.8}$	1~400
Pyrenees, Spain	A	$I = 17.96 \times D^{-0.59}$	> 168
Apuane Alps, Tuscany, Italy	Sh	$Lower\ threshold: I = 26.871 \times D^{-0.638}$ $Upper\ threshold: I = 85.584 \times D^{-0.781}$	0.1~35
N of Lisbon, Portugal	A	$I = 84.3 \times D^{-0.57}$	0.1~2000
Indonesia	D	$I = 92.06 - 10.68 \times D$	2~4

Note: Landslides type - Sh, shallow landslide; D, debris flow; A, all types.

As indicated in Table 2 and Figure 2, shallow landslides can be triggered by lower intensity or shorter duration during rainfall events, comparing to other types of landslides. The lower bound of the thresholds is the combination of World-Sh and Vancouver-Sh. The zone under the lower bound is the low-risk zone for shallow landslides. The upper bound of the thresholds is composed of three lines: Apuane Alps-Sh(Upper), Taiwan-A, and Lisbon-A. The zone above the upper bound has extremely high risk for shallow landslides. The threshold of debris flow in Indonesia also locates in this zone. The zone in between is considered as the high-risk zone.

3 NUMERICAL MODELING STRATEGY

Rainfall weakens an earth slope mainly in three ways: it increases the water content in the soil, thereby reduces the apparent cohesion, c_a; downhill frictional drag on the slope, creating a destabilizing effect; discharge as a surface runoff and erodes the slope (Borja, 2010). Therefore, unsaturated soil behavior and fluid-solid coupling effect are required to consider in the modelling.

3.1 Unsaturated soil behavior and parameters

Matric suction, $s=u_a-u_w$, is the independent variable which has significant influence on seepage and deformation behavior of unsaturated soils. The key properties include effective stress, yield surface, and permeability coefficient in unsaturated state.

Although the two-independent variable concept has been proposed for a long time, Bishop's effective stress is widely utilized for unsaturated soil modeling, as indicated by,

$$\sigma' = (\sigma - u_a) + \chi(u_a - u_w) \quad (1)$$

where, σ' is the effective stress, u_a and u_w are pore air pressure and pore water pressure, respectively; χ is the matric suction coefficient which varies from 0 to 1 covering the range from dry to fully saturated conditions. χ is often assumed to be equal to the degree of saturation, S_r.

The yield surface of unsaturated soils can be extended from classical Mohr-Coulomb theory by introducing the matric suction, (u_a-u_w), as indicated in (2).

$$\tau_f = c' + (\sigma - u_a)\tan\varphi' + (u_a - u_w)\tan\varphi_b \quad (2)$$

where, φ_b is the angle indicating the rate of increase in shear strength with respect to a change in matric suction, (u_a-u_w). The value of φ_b appears to be consistently equal or less than φ', and ranges in 7~25.5° according to available testing results (Fredlund, 2012). The apparent cohesion can be expressed by,

$$c_a = c + (u_a - u_w)\tan\varphi_b \quad (3)$$

The formula (3) indicates that, the apparent cohesion decreases with the matric suction.

Figure 3 shows the typical stress path of soils in shallow depth during infiltration under rainfall. As water content increases, the Mohr circle reduces from the large dash circle to the small one. However, the soil still reaches its critical state due to the reduction of

apparent cohesion. The plastic flow after yielding leads to large superficial slope movements.

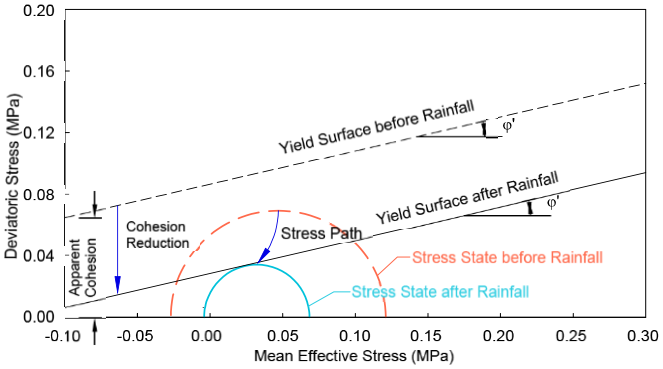

Fig. 3 Stress path and yield surface moving during rainfall events (Jamei, 2015)

In terms of hydraulic behavior, unsaturated soil has lower permeability coefficient, since air occupies part of void in between soil particles. The permeability coefficient is usually expressed as a relative value based on the permeability coefficient in saturated state and the matric suction (or negative pore pressure alternatively). The van Genuchten (1980) model is the most widely accepted hydraulic model, which is indicated in (4).

$$k_r = \begin{cases} \frac{\left[1-|\alpha h|^{n-1}(1+|\alpha h|^n)^{-m}\right]^2}{(1+|\alpha h|^n)^{m/2}} & h \le 0 \\ 1 & h > 0 \end{cases} \quad (4)$$

where, h is the negative pore pressure head, h=-p/γ_w; α is the parameter related to the air entry pressure; m=1-1/n; Table 3 lists the fitted van Genuchten model parameters, n and α based on 72 samples collected from literature (Ghanbarian, 2010).

Table 3 Typical values of the parameters n and α

Material	Clay Content (g/kg)		n		α (m^{-1})	
	Min	Max	Min	Max	Min	Max
Sand	14	18	2.22	2.56	2.74	2.65
Loamy sand	23	108	1.33	2.56	4.41	2.35
Sandy loam	70	178	1.12	2.38	4.90	1.27
Sandy clay loam	208	349	1.06	1.85	3.92	1.47
Loam	122	260	1.23	1.96	4.90	1.76
Silt loam	120	270	1.14	1.25	9.60	1.47
Silty clay loam	280	390	1.14	1.43	8.82	0.98
Clay loam	304	348	1.05	1.64	4.90	0.78
Sandy clay	352	421	1.10	1.49	4.90	1.76
Silty clay	420	460	1.09	1.10	6.37	5.39
Clay	452	452	1.51	1.51	0.88	0.88

It can be observed that, both the mechanical and hydraulic models of unsaturated soils are based on matric suction, which can be estimated by soil water characteristic curves (SWCCs). The SWCCs correlates the matric suction, (u_a-u_w), and water content in soils.

The measurement of SWCC data in the laboratory is time-consuming and costly. Alternatively, SWCC can be estimated by using physical properties such as particle size distribution (PSD), liquid limit (LL), plastic limit (PL), when the test result is unavailable (Hernandez, 2011). The widely adopted SWCC model proposed by Fredlund and Xing (1994) is,

$$S_r = C(\Psi)\left[\frac{1}{\left\{\ln\left[e+\left(\frac{\Psi}{a_f}\right)^{b_f}\right]\right\}^{c_f}}\right] \quad (5)$$

$$C(\Psi) = 1 - \frac{\ln\left(1+\frac{\Psi}{h_r}\right)}{\ln\left(1+\frac{1000000}{h_r}\right)} \quad (6)$$

The parameters, a_f, b_f, c_f, and h_r. can be obtained by (7)-(10),

$$a_f = 10^{\left(0.69-\frac{2.7}{1+e^{(4-0.14GI)}}\right)} \quad (7)$$

$$b_f = 10^{\left(\frac{0.78}{1+e^{(6.75-0.19GI)}}\right)} \quad (8)$$

$$c_f = 0.03 + 0.62 \times \mathrm{e}^{\left(-0.82(\log a_f - 0.57)^2\right)} \quad (9)$$

$$h_r = 494 + \frac{660}{1+e^{(4-0.19GI)}} \quad (10)$$

In (7)-(10), the group index (GI) can be calculated by,

$$GI = (P_{200}-35)[0.2+0.005(LL-40)] + 0.01(P_{200}-15)(PI-10) \quad (11)$$

where, P_{200} is the passing the No. 200 sieve; LL is the liquid limit; PI is the plastic index.

The weighted plastic index, wPI, is:

$$wPI = \frac{P_{200}\times PI}{100} \quad (12)$$

3.2 Fluid-solid coupling method

Analysis that couples the seepage and stress can be implemented in various ways. The simplest way is to obtain the pore water pressure distribution by conducting seepage analysis firstly, then incorporate it into the following stress analysis by introducing pore water pressure. Such method is the so-called semi-coupled analysis. However, since deformation due to stress analysis does not influence the seepage phenomenon inversely, this method may lead to unacceptable deviation from real situations.

Fluid-solid fully-coupled analysis is the two-way coupled method between seepage and solid stress. This method does not follow assumption that steady state pore water pressure is maintained. Hence, it is suitable for simulating the transient seepage phenomenon.

Furthermore, comparing to the consolidation analysis, it is possible to define the changes in seepage boundary conditions with time, boundary flow rate etc. These are necessary in the modelling of rainfall-induced slope movement.

4 ASSESSMENT PROCEDURE

The influence of rainfall-induced slope movements can be assessed in two major steps: preliminary assessment; and strain-based design analysis, based on data collection. The design of remediation plan can be incorporated in the assessment procedure. This procedure is illustrated in Fig. 4.

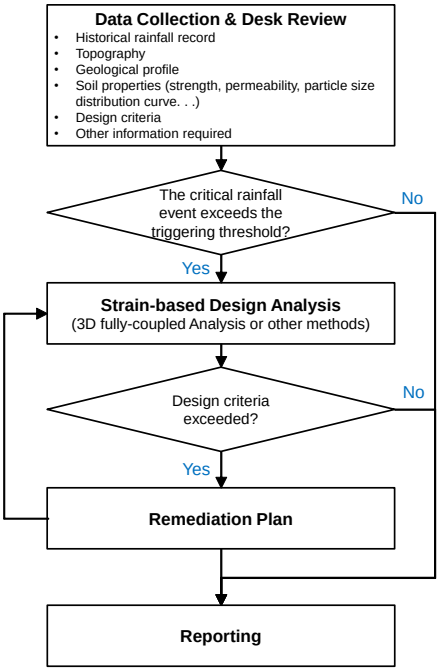

Fig. 4 Assessment procedure of rainfall-induced slope movement

Note that collected data should be sufficient to estimate the unsaturated soil parameters for strain-based design analysis. The minimum requirements of the parameter estimate include PSD, liquid limit, and plastic limit. For concave slope, real topography needs to be modelled in 3D to consider the influence of larger catchment area.

5 CASE STUDY

5.1 Brief introduction

A concave slope in Brisbane area, Australia, embedded with utility service pipelines was under concern due to historical shallow landslides and damage to the services. As per design rainfall depth chart by Queensland government (Fig. 5), 1-day rainfall depth for 50% annual exceedance probability (AEP) is approximately 70mm, which is 3mm/hr in intensity. This indicated that the location was in the high-risk zone of shallow landslides, thus strain-based design analysis was required. In the following analysis, 5% AEP rainfall intensity (150mm/day) with 3-day duration (1 in 2000 AEP) was adopted to cover the potential risk.

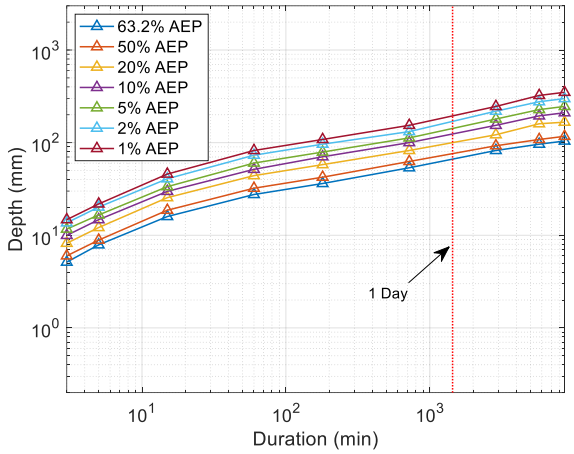

Fig. 5 Design rainfall depth chart in the location

The geological profile was conservatively simplified to a 4-layer stratum: 4.0m colluvium, 4.0m XW basalt, 10.0m HW basalt, and bedrock. The ground surface of the model was generated in MIDAS GTS NX using borehole elevation records, as illustrated in Fig.6. The model is 260m in length and 150m in width, with the pipeline incorporated.

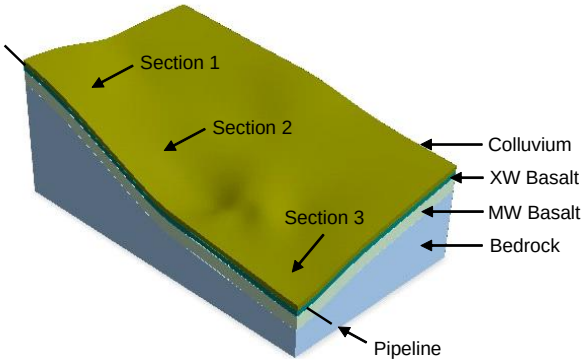

Fig. 6 3D geometry of the assessed area

5.2 Properties of the colluvium

Slope movement or shallow landslides were expected to occur within the colluvium of 4m in thickness, which was considered as the key layer. The colluvium in this area is typically comprised of very stiff to hard clay. SPT N values in the colluvium varies between 23 and 37. The liquid limit and plasticity limit are 43% and 35%, respectively. The typical PSD data of the colluvium is indicated in Fig.7.

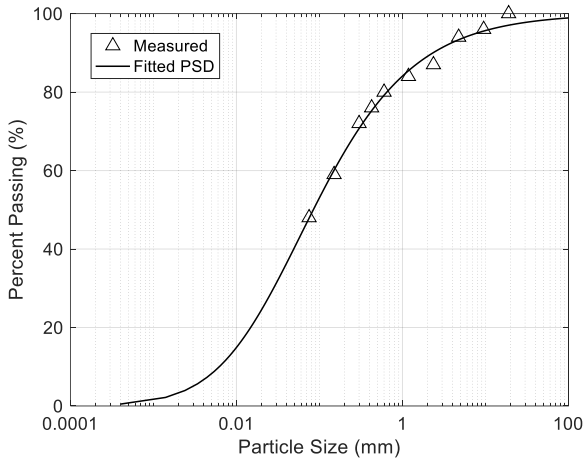

Fig. 7 Particle size distribution curve of the colluvium

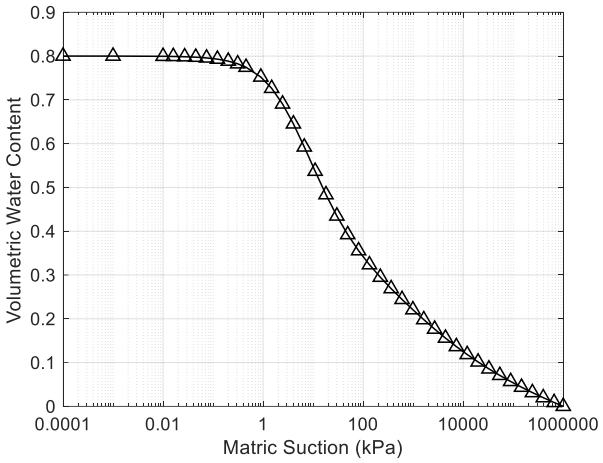

Fig. 8 Estimated SWCC of the colluvium

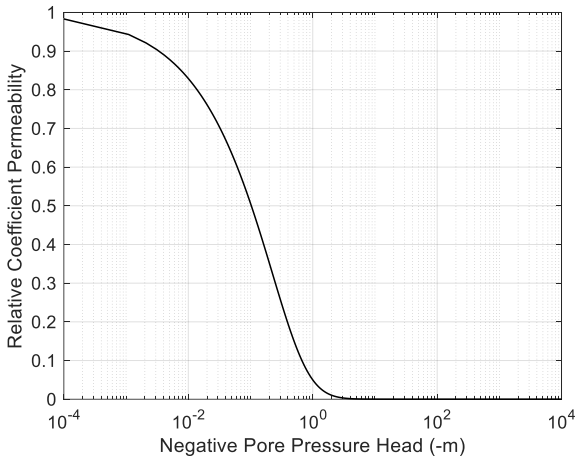

Fig. 9 Estimated relative permeability coefficient, k_r

The SWCC of the colluvium was estimated by using the PSD and Atterberg limits, as illustrated in Fig.8. Taking the parameters, α=0.88 and n=1.51, for clay in Table 3, then the relative coefficient permeability was estimated and plotted in Fig. 9. The saturated permeability coefficient, k_s, is 2.0×10^{-7}cm/s for horizontal and 1.0×10^{-7}cm/s for vertical.

5.3 Calculated slope movement under rainfall

The contour of the slope movement was obtained from the 3D fully-coupled numerical analysis, as shown in Fig. 10. The results indicated a maximum 1.114m superficial movement occurred due to the intense rain. The calculated movement is in accordance with measured in recent shallow moving events.

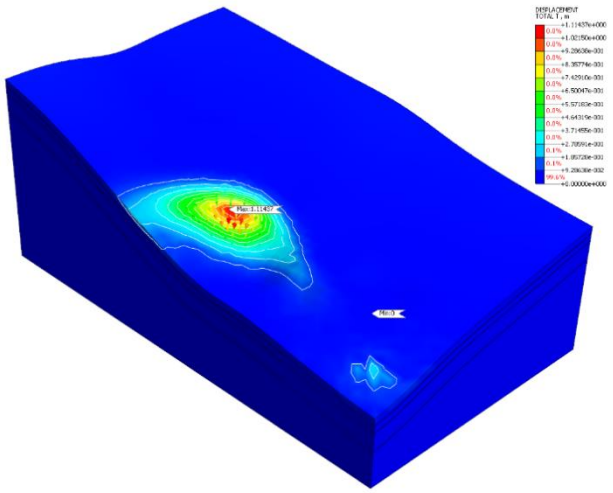

Fig. 10 Slope superficial movement at the end of the rainfall

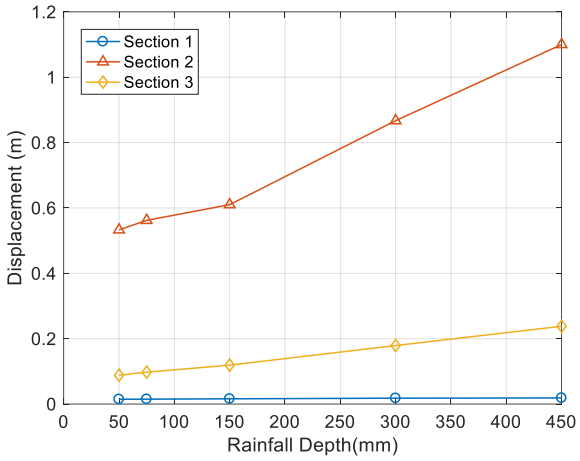

Fig. 11 Development of slope movement at three sections along the pipeline

The slope movements at three sections (see in Fig.6) along the pipeline were extracted from the 3D models. Development of the movements were plotted in Fig. 11. The maximum movement occurred in section 2 (central section), and the minimum one can be found in section 1 (upper section). Saturated zone was formed after 1-day rainfall which accelerated the moving rate in section 2. In addition, three movement trends indicated that the superficial movement tended to occur in short duration under intense rain. However, the intensity which triggers the movements has not been studied in this project.

As indicated in Fig. 12, the flow path of water during the rainfall event clearly showed the rainfall-induced surface seepage. Comparing to convex slopes and highway slopes, this concave slope has significantly larger catchment area. This type of topography has higher chance to trigger large slope movement or shallow landslides. 3D strain-based numerical model is required to be adopted for assessment purpose.

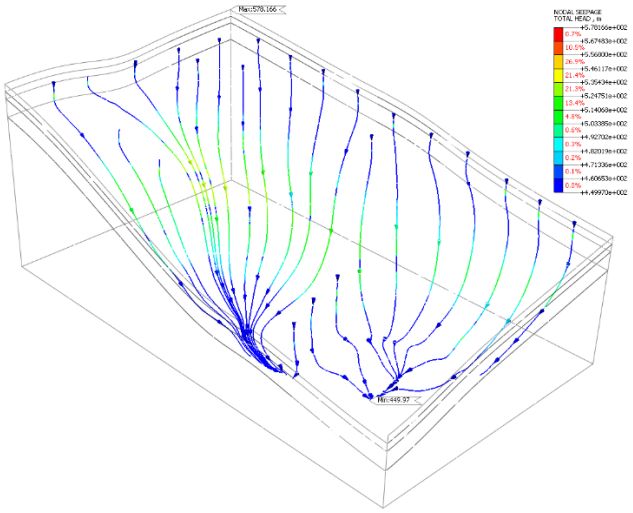

Fig. 12 Flow path of water during the rainfall event

5.4 Risk remediation plan

Two remediation options were proposed in this project: scenario 2 – removal of the colluvium in section 2; scenario 3 – install finger drains in section 1 and replace colluvium in section 3 with free drainage material based on scenario 2. The original geometry is the scenario 1.

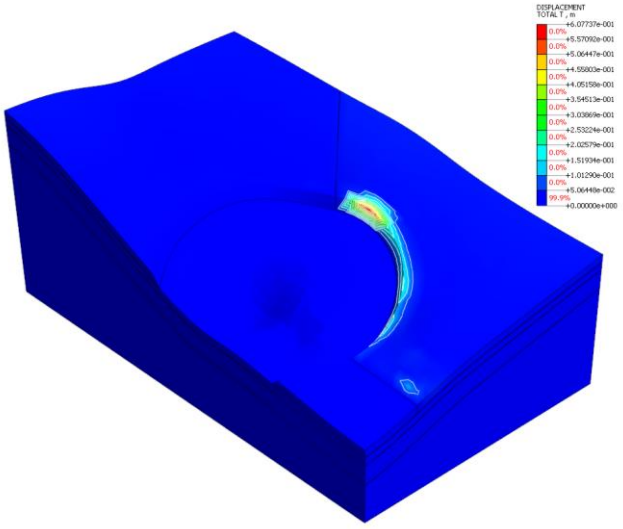

Fig. 13 Slope movement after remediation (Scenario 3)

Fig.13 showed the slope movement contour after remediation of scenario 3. Figure 14 compared movement reduction at three sections in two remediation scenarios. It can be observed that, the movements in section 2 was completely eliminated as the colluvium is removed, and displacement in section 1 and 3 were significantly reduced. The scenario 3 has greater displacement reduction than scenario 2.

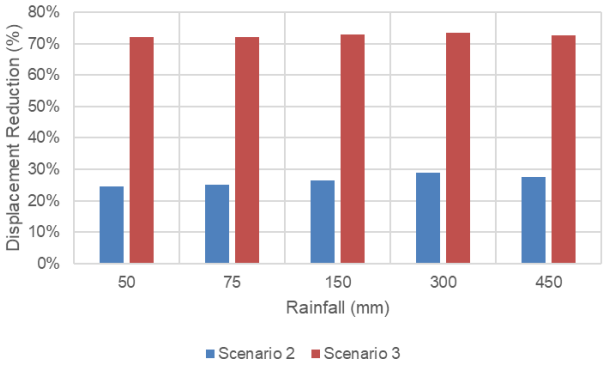

(*a*)

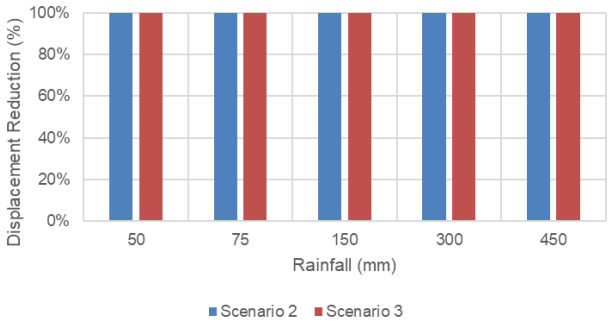

(*b*)

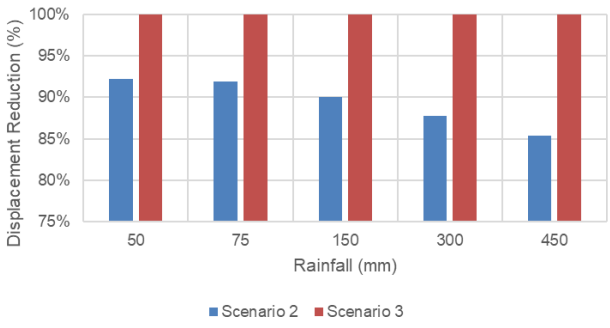

(*c*)

Fig. 14 Displacement reduction in each remediation scenario

In addition, a pipeline element was incorporated in the scenario 3 model. Pipe-soil interaction was considered by using the pile elements provided in MIDAS GTS NX. The results showed the maximum 2.4cm displacement was induced by slope movement with remediation. This is a tolerable pipeline displacement as advised by pipeline structural engineers.

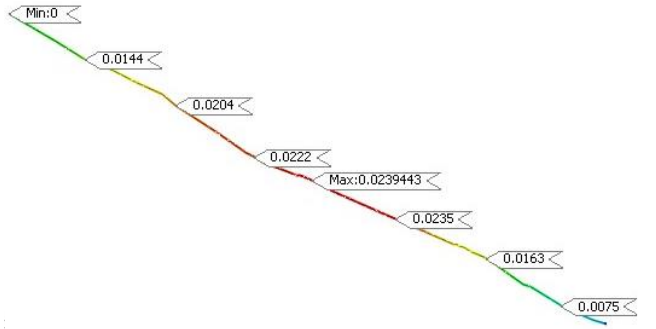

Fig. 15 Pipeline displacement after remediation (Scenario 3)

6 CONCLUSIONS

The conclusions can be drawn as follows:

⑴The 2-step procedure of assessing the influence of rainfall-induced slope displacement & shallow landslides was proposed and justified in industry. The relevant assessing methods were also introduced in detail. These provide a reference for the problem of slopes with displacement-sensitive structures embedded.

⑵The 3D effect of concave slopes is significant due to the large catchment area, which is illustrated in the case study. The topography of slope needs to be considered in the strain-based design analysis.

⑶Unsaturated soil properties are the key in the rainfall-induced slope displacement analysis. Attention should be paid to meet the minimum requirement of data collection, which is inclusive of PSD, LL, and PL.

ACKNOWLEDGMENTS

We are grateful to our colleagues who helped us in the discussion and design stages.

REFERENCES

Au, S. W. C. (1998). Rain-induced slope instability in Hong Kong. *Engineering Geology*, 51, 1–36.

Borja, R. I., & White, J. A. (2010). Continuum deformation and stability analyses of a steep hillside slope under rainfall infiltration. *Acta Geotechnica*, 5, 1–14.

Brand E. W., Premchitt J., & Phillipson H. B. (1984). Relationship between rainfall and landslides in Hong Kong. *In Proceedings, 4th International Symposium on Landslides* (pp. 377–384). Toronto.

Cai, F., Ugai, K., Wakai, A., & Li, Q. (1998). Effects of horizontal drains on slope stability under rainfall by three-dimensional finite element analysis. *Computers & Geotechnics*, 23(4), 255-275.

Caine, N. (1980). The rainfall intensity - duration control of shallow landslides and debris flows. *Geografiska Annaler*, 62(1/2), 23-27.

Capparelli, G., Iaquinta, P., Iovine, G. G. R., & Versace, P. (2012). Modelling the rainfall-induced mobilization of a large slope movement in northern calabria. *Natural Hazards*, 61(1), 247-256.

Chen, Q., Han J., Ai K. (2004) Monitoring and analysis of slope deformation along a speedway. *Chinese Journal of Rock Mechanics and Engineering*, 23(2): 299-302

Chen, C. Y., Chen, T. C., Yu, F. C., Yu, W. H., & Chun-Chieh, T. (2005). Rainfall duration and debris-flow initiated studies for real-time monitoring. *Environmental Geology*, 47(5), 715-724.

Cho S.E., Lee S.R. (2001). Instability of unsaturated soil slopes due to infiltration. *Computers and Geotechnics*, 28(3), 185-208.

Fredlund, D. G., & Xing, A. (1994). Equations for the soil-water characteristic curve. *Canadian Geotechnical Journal*, 31(4), 521-532.

Fredlund, D. G. (2012). Unsaturated Soil Mechanics in Engineering Practice. *John Wiley & Sons.*

Genuchten, M. T. V. (1980). A closed-form equation for predicting the hydraulic conductivity of unsaturated soils. *Soil Science Society of America Journal*, 44(44), 892-898.

Ghanbarian-Alavijeh, B., Liaghat, A., Genuchten, M. T. V. (2010). Estimation of the van genuchten soil water retention properties from soil textural data. *Pedosphere*, 20(4), 456-465.

Guzzetti, F., Peruccacci, S., Rossi, M., & Stark, C. P. (2007). Rainfall thresholds for the initiation of landslides in central and southern europe. *Meteorology & Atmospheric Physics*, 98(3-4), 239-267.

Hernandez, G. T., Zapata, C., Chair, S., Houston, M., & Witczak. (2011). Estimating the soil–water characteristic curve using grain size analysis and plasticity index. Thesis: Arizona State University

Jamei, M., Guiras, H., Ben Hamouda, K., Hatira, M., & Olivella, S. (2008). A study of the slope stability in unsaturated marly clay soil. *Studia Geotechnica et Mechanica*, 95–106

Jamei, M., Guiras, H., & Olivella, S. (2015). Analysis of slope movement initiation induced by rainfall using the elastoplastic barcelona basic model. *European Journal of Environmental and Civil Engineering*, 19(9), 1033-1058.

Lateh, H., Muhiyuddin, W. M., Taib, B., & Khan, Y. A. (2010). Monitoring of hill-slope movement due to rainfall at gunung pass of cameron highland district of peninsular malaysia. *International Journal of Earth Sciences & Engineering*, 03(1), 974-5904.

Lim, T. T., Rahardjo, H., Chang, M. F., & Fredlund, D. G. (1996). Effect of rainfall on matric suctions in a residual soil slope. *Canadian Geotechnical Journal*, 33, 618–628.

Muntohar, A. S., & Liao, H. J. (2010). Rainfall infiltration: infinite slope model for landslides triggering by rainstorm. *Natural Hazards*, 54(3), 967-984.

P. Orense, R., Shimoma, S., Maeda, K., & Towhata, I. (2004). Instrumented model slope failure due to water seepage. *Journal of Natural Disaster Science*, 26(1), 15-26.

Pinto, P. S. S. E., Barradas, J., & Sousa, A. (2011) Lessons learned from case histories on landslides.. Geotechnical Engineering *For Disaster Mitigation And Rehabilitation And Highway Engineering 2011: Geotechnical and Highway Engineering — Practical Applications, Challenges and Opportunities*: 54-73

Qian J.Y., Zhang G., Zhang J.M. (2011) Centriguge model tests for deformation mechanicsm of soil slope during rainfall. *Rock and Soil Mechanics*, 32(2): 398-403

Sagitaningrum, F. H., & Bahsan, E. (2017). Parametric study on the effect of rainfall pattern to slope stability. MATEC Web of Conferences, 101, 05005. DOI: 10.1051/matecconf/201710105005

Van Sint Jan M, Talloni P (1993) Flujo de sedimentos del 18 de Juniode 1991 en Antofagosta: La Serena, Chile. *Tercer Congreso Chileno de Ingenieria Geotecnia* 1:247–265

Zhan, L. T., Liu, X. C., Pei, T., & Chen, Y. M. (2014). Centrifuge modelling of rainfall-induced slope failure in silty soils and validation of intensity-duration curves. *Chinese Journal of Geotechnical Engineering*, 36(10), 1784-1790.